iScience

Article

Imaging lipid rafts reveals the principle of ApoE4-induced Aβ upregulation in human neurons

Graphical abstract

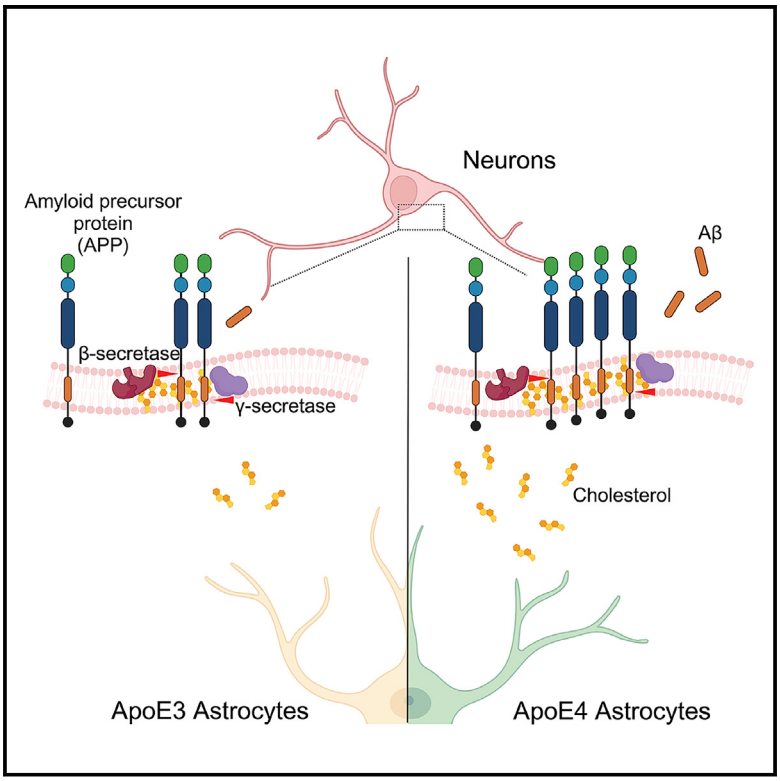

Highlights

- Simultaneous imaging of lipid rafts and proteins in neurons with ToF-SIMS
- Cholesterol enhances APP processing and expands lipid raft domains in human neurons
- ApoE4 astrocytes increase APP expression within neuronal lipid raft domains
- $A\beta_{42}$ upregulation by ApoE4 astrocytes is clathrin-mediated endocytosis independent

Authors

Se-In Lee, Heejin Lim, Na Yeon Kim, ..., Hyein Lee, Dae Won Moon, Jinsoo Seo

Correspondence

dwmoon@dgist.ac.kr (D.W.M.), jsseo@dgist.ac.kr (J.S.)

In brief

Natural sciences; Biological sciences; Neuroscience; Cellular neuroscience; Techniques in neuroscience

Lee et al., 2025, iScience *28*, 111893
February 21, 2025
https://doi.org/10.1016/j.isci.2025.111893

CellPress

iScience

CellPress
OPEN ACCESS

Article

Imaging lipid rafts reveals the principle of ApoE4-induced Aβ upregulation in human neurons

Se-In Lee,[1,5] Heejin Lim,[2,3,5] Na Yeon Kim,[1] Jichang Yu,[1] Joonho Cho,[1] Hyein Lee,[1] Dae Won Moon,[2,*] and Jinsoo Seo[1,4,6,*]
[1]Department of Brain Sciences, Daegu Gyeongbuk Institute of Science & Technology, Daegu 42988 South Korea
[2]Department of New Biology, Daegu Gyeongbuk Institute of Science & Technology, Daegu 42988 South Korea
[3]Center for Scientific Instrumentation, Korea Basic Science Institute, Cheongju 28199 South Korea
[4]Center for Synapse Diversity and Specificity, Daegu Gyeongbuk Institute of Science & Technology, Daegu 42988 South Korea
[5]These authors contributed equally
[6]Lead contact
*Correspondence: dwmoon@dgist.ac.kr (D.W.M.), jsseo@dgist.ac.kr (J.S.)
https://doi.org/10.1016/j.isci.2025.111893

SUMMARY

Lipid rafts in plasma membranes are thought to provide a platform for regulating signaling pathways by increasing the expression or proximity of proteins in the same pathway. Despite this understanding, the absence of direct, simultaneous observations of lipid rafts and their affiliated proteins has hindered a comprehensive assessment of their roles across various biological contexts. Amyloid-β (Aβ), a hallmark of Alzheimer's disease (AD), is generated from the sequential cleavage of amyloid precursor proteins (APPs) by β- and γ-secretases, primarily within endosomes after APP endocytosis by canonical clathrin-mediated endocytosis in neurons. In this study, we developed a protocol for imaging APP on lipid rafts using time-of-flight secondary ion mass spectrometry (ToF-SIMS) and found that astrocyte ApoE4 contributes to an increase in APP localization on lipid rafts, subsequently elevating $A\beta_{42}$ synthesis in a clathrin-independent manner in neurons.

INTRODUCTION

When the "fluid mosaic model," the existence of restricted domains with lipid and protein complexes in cellular membranes, was first devised in 1972,[1] the detergent-resistant fractions separated from detergent-labile fractions were soon experimentally observed.[2] Since then, better evidence has arisen from the visualization of this structure, which is dependent on advances in techniques and tools for imaging. Restricted areas in the membrane consist of cholesterol and saturated lipids that form unique and packed domains called "lipid rafts".[3] This domain provides space for recruiting specific lipids and proteins that synergistically or sequentially regulate specific cellular signaling pathways.[4]

Lipid rafts are defined as heterogeneous, cholesterol-rich dynamic domains that span approximately 10–200 nm but have the potential to expand with dynamic properties.[4,5] However, the presence and nature of this structure remain controversial owing to the limited evidence of direct imaging of this dynamic lipid-protein complex structure in living cells. Although current single-cell mass measurements provide a discrimination index for protein and lipid masses based on either methyl or methylene signals, the spatial information is limited, even under live conditions.[6] Furthermore, measuring reference molecules representing proteins or lipids cannot provide information on the individual metabolites/proteins of interest.[6] We recently devised a protocol for imaging various fatty acids and cholesterol in the plasma membranes of live cells in a culture solution.[7] Although this approach visualizes the cluster of cholesterol-rich platforms considered to be lipid rafts, more evidence, such as colocalization with other components known to be exclusively localized to lipid rafts, is required. In this study, we revised the previous protocol for imaging the colocalization of specific lipids and proteins at the single-cell level and identified the distribution of lipid rafts and associated proteins.

The physiological roles of lipid rafts are not limited to providing a structural platform for membrane-bound proteins, as they can actively regulate specific signaling pathways in an orchestral manner.[4,8] Proteins anchored by glycosylphosphatidylinositol (GPI) or palmitoylated are known to be raftophilic.[4] A previous study showed that GPI-anchoring in β-secretase 1 (BACE1) induces its localization to lipid rafts and is positively correlated with amyloid precursor protein (APP) processing and generation of amyloid-β (Aβ), a peptide that plays a central role in the pathology of Alzheimer's disease (AD).[9] APP is also known to be palmitoylated, which increases with age.[10] APP palmitoylation facilitates its localization to lipid rafts and results in Aβ production.[10] Therefore, limiting localization of BACE1 or/and APP to lipid rafts may be an efficient strategy for reducing aberrant Aβ generation.

Changes in cholesterol were shown to impact APP and BACE1 localization in lipid rafts.[11–13] We previously reported an increase in the expression of membrane cholesterol and APP, resulting in increased Aβ production in human neurons cultured with conditioned media from astrocytes carrying *APOE4*, the strongest genetic risk factor for late-onset AD.[14] However, direct evidence for the APP localization to lipid rafts in these conditions was not provided. In this study, we visualized lipid rafts at the single-cell level with the time-of-flight secondary ion mass spectrometry (ToF-SIMS) in neurons differentiated from human-induced pluripotent stem cells (hiPSCs) and determined the differential effects of the *APOE4* variants with the Swedish mutant (KM670/671NL) in *APP* causing familial AD on APP translocation to lipid rafts and its processing.

RESULTS

Imaging lipid rafts in the neuronal plasma membrane by ToF-SIMS

We have previously shown that keeping cells alive with single-layer graphene is critical for imaging intact cholesterol in the membrane.[7] Since a fixation step is required to image fluorescence-tagged proteins, we modified our previous protocol by performing immunostaining without permeable agents, such as detergents, and adding an air plasma cleaning step instead of a graphene covering, followed by imaging within 2 h. We confirmed that cholesterol images from the modified protocol showed patterns similar to those from live neurons and caused neither signal distortion nor microcracks (Figures 1A and 1B).

Flotillin-1 is known to be present in the detergent-resistant domain of the plasma membrane and is, therefore, considered a marker for lipid rafts.[15] As cholesterol is the major lipid component of lipid rafts, we aimed to detect flotillin-1 and cholesterol double-positive signals to image lipid rafts. To simultaneously image the lipids and proteins in the same sample, we used the ToF-SIMS tool. We have previously shown that the conjugation of metal oxide nanoparticles to antibodies allowed us to image proteins using SIMS.[16] Quantum dots (QDs) are fluorescent nanoparticles that can be detected using both confocal microscopy and ToF-SIMS.[17] To image the lipid rafts in the human neuronal plasma membrane, we differentiated hiPSCs derived from healthy individuals into cortical excitatory neurons and maintained them in hiPSC-derived astrocyte-conditioned media (ACM), as previously described[14] (Figures S1A–S1C).

To specifically detect membrane-bound flotillin-1, we first conjugated an anti-flotillin-1 antibody with biotin and treated them with neurons (Figure S1D). Neurons were then lysed and pulled down with streptavidin beads to confirm the labeling of membrane-bound flotillin-1 (Figure S1E). To image membrane flotillin-1, we linked the QDs and streptavidin and incubated them with biotinylated flotillin-1 antibody to generate the "antibody-biotin-streptavidin-QD" complex (Figure S1F). Both confocal microscopy and transmission electron microscopy (TEM) confirmed that membrane flotillin-1 could be labeled by QDs (Figures S1G and S1H). However, no clear QD signal was observed when this sample was subjected to ToF-SIMS imaging (Figure S1I). We speculated that the secondary ions generated from the QDs could be diluted by negatively charged carbohydrates conjugated to membrane-bound molecules through glycosylation. To test this hypothesis, we treated the QD-labeled neurons with glycosidases (both N- and O-glycosidases) before secondary fixation for ToF-SIMS (Figure 1A). We found that removing carbohydrates significantly improved the QD signals from ToF-SIMS (Figure 1B). As glycolipids and GPI-anchored proteins are known to be enriched in lipid rafts, these data further suggest that QD-labeled flotillin-1 is mainly located in lipid rafts. We confirmed that our protocol applies to other membrane-bound proteins, such as APP and BACE1 (Figures 2C and S1J).

After ToF-SIMS imaging in the spectrometry mode with a beam size of 3 μm from 38.4 × 38.4 μm^2 (resolution of 128 × 128 pixels) for single-cell analysis (Figure 1C), we determined the Pearson's correlation coefficient between the signals from cholesterol and flotillin-1. We used a 50% peak amplitude threshold to eliminate the potential contribution of the cell shape-dependent increase in the membrane content signals. We found that the index of intensity difference for cholesterol and flotillin-1 was lower than that for cholesterol and phosphocholine (Figure 1D). The expression patterns of cholesterol and flotillin-1 were significantly correlated. However, the expression profile of phosphocholine, a major derivative of phosphatidylcholine that is not lipid raft specific, did not show a positive correlation with cholesterol expression (Figure 1E).

Cholesterol positively regulates APP processing and lipid raft territory in human neurons

Cholesterol regulation has been suggested to modify lipid rafts. Cholesterol depletion by methyl-β-cyclodextrin (MβCD) has been shown to reduce the levels of membrane cholesterol-enriched areas thought to be lipid rafts, as detected by the cholera toxin-B labeling of ganglioside GM1.[7,14] In contrast, increased levels of extracellular cholesterol have been shown to expand the lipid raft domains in the membrane.[11,14] We treated human neurons with either cholesterol or MβCD and examined the changes in the expression profiles of membrane flotillin-1 and cholesterol (Figure 2A). Consistently, we found that cholesterol treatment increased, but MβCD treatment reduced the neuronal membrane cholesterol and flotillin-1 levels without changing the size of the cells (Figures S2A–S2G). Plotting the distribution of the percentage of pixel number as a function of signal intensity showed that this change was caused not only by an expansion of the signal-positive area but also by an increased density of signals (Figures S2E and S2G). The colocalization analysis showed that the lipid raft domain was expanded in cells by cholesterol treatment but shrunken by MβCD treatment (Figures S2H and S2I). As well documented[18] and as we observed (Figures 1D and 2E), cholesterol has a high affinity for lipid rafts. However, cholesterol is also present in non-raft membranes. Therefore, external cholesterol may also be incorporated into non-raft fractions. We examined cholesterol changes in flotillin-1-negative areas in the cholesterol images and found no differences from the control following cholesterol or MβCD treatment (data not shown). This suggested prolonged treatment with cholesterol or MβCD (four days and one day, respectively) has significantly and specifically impacted lipid rafts.

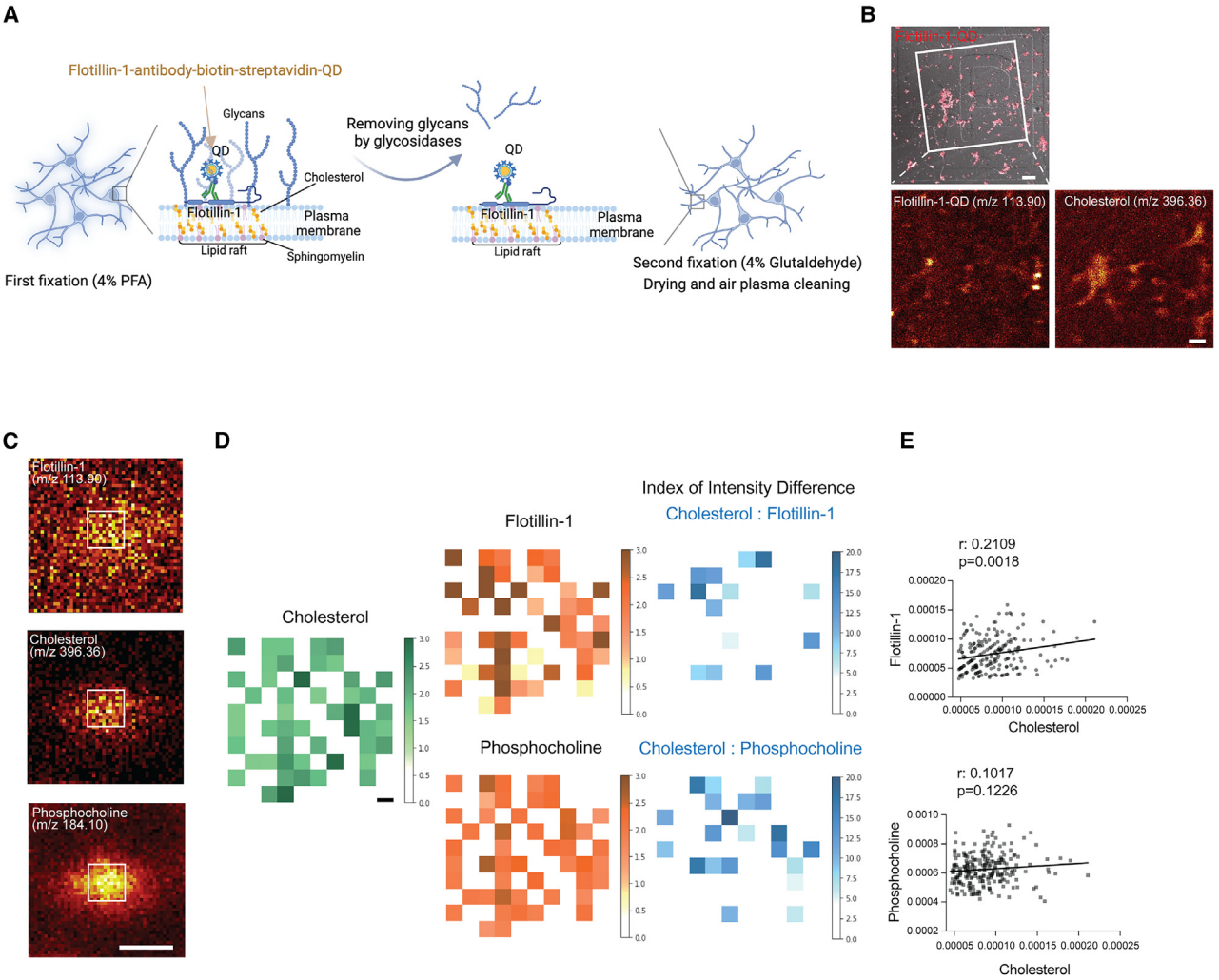

Figure 1. Imaging lipid rafts in the neuronal plasma membrane by ToF-SIMS

(A) Schematics for imaging of flotillin-1 in the plasma membrane with QDs.

(B) Confocal microscope images (top) and ToF-SIMS images (bottom) from hiPSCs-derived neurons treated with QD-conjugated anti-flotillin-1 antibody. All images were obtained from the same area. Scale bars, 50 μm.

(C) ToF-SIMS images from a single neuron labeled with QD-conjugated anti-flotillin-1 antibody. Scale bars, 5 μm.

(D) The index of intensity difference for cholesterol and flotillin-1, or cholesterol and phosphocholine, was calculated (as described in STAR Methods) and visualized. The y axis indicates the intensity of the pixel (a.u.). Scale bars, 600 nm.

(E) The Pearson's correlation coefficient between cholesterol and flotillin-1 or cholesterol and phosphocholine. (n = 5 experiments from 3 independent cultures).

Studies have shown that increased levels of extracellular cholesterol positively regulate APP processing in *in vitro* and *in vivo* models, potentially by recruiting membrane-bound APPs to lipid rafts.[11,14,19] We repeatedly observed reduced secretions of both $A\beta_{40}$ and $A\beta_{42}$ from neurons after treatment with MβCD (Figures 2A and 2B). When treated with cholesterol, the neurons secreted more $A\beta_{42}$; however, the $A\beta_{40}$ levels were comparable to controls (Figure 2B). To directly monitor APP dynamics in the membrane upon extracellular cholesterol regulation, we prepared the "APP antibody-biotin-streptavidin-QD" complex (Figures S1K and S1L) and treated to human neurons for ToF-SIMS imaging. We confirmed its specificity for APP detection using confocal microscopy with another APP antibody visualized using a fluorescent secondary antibody (Figure S1M). To validate that the signals were from membrane-bound proteins, we targeted mitofusin-1 (Mfn1), which is specifically expressed in the outer membrane of mitochondria. With the "Mfn1 antibody-biotin-streptavidin-QD," we could not detect any signals by TEM unless we added an additional step to permeabilize the cell membrane (Figure S1N). These data show that the signals from our protocol were specific for membrane proteins.

ToF-SIMS imaging showed upregulated APP signals in the membrane upon cholesterol treatment (Figures 2D and 2E), and the distribution pattern of pixels at different intensities showed that the increased signals were not simply due to the

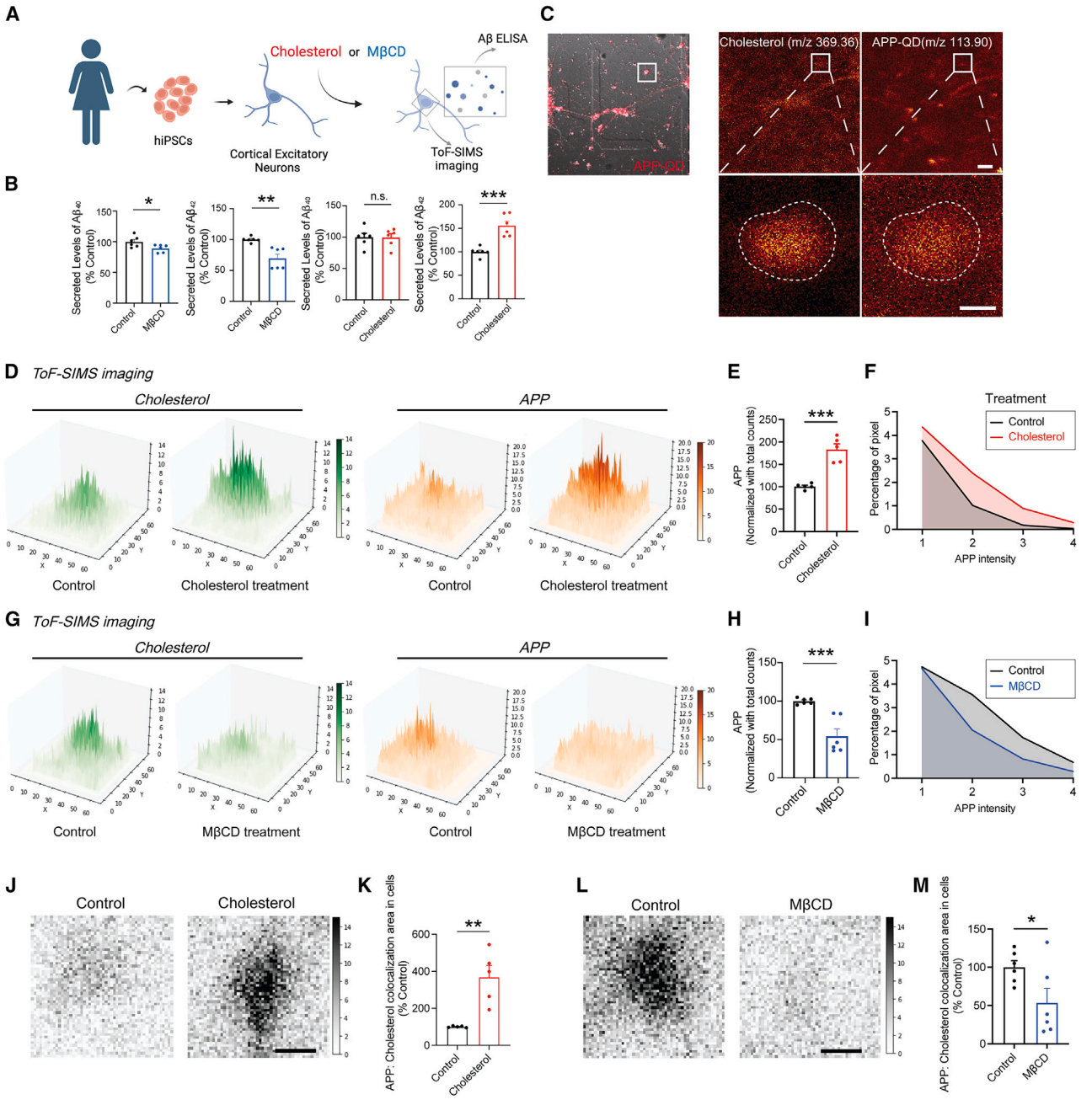

Figure 2. Cholesterol positively regulates amyloidogenic APP processing and lipid raft territory in human neurons

(A) Schematics for the experiments to determine the effects of cholesterol levels on APP processing and lipid rafts.

(B) Levels of secreted $A\beta_{40}$ and $A\beta_{42}$ from neurons were measured by ELISA. (6 independent cultures).

(C) Confocal microscope images (left) and ToF-SIMS images (middle, right) from hiPSCs-derived neurons treated with QD-conjugated anti-APP antibody. All images were obtained from the same area. Scale bars, 50 μm (top), 10 μm (bottom).

(D) 3D plot of ToF-SIMS images from control and cholesterol-treated hiPSCs-derived neurons. The y axis indicates the intensity of the pixel. (a.u.).

(E and F) Pixel counts for APP normalized by total counts (E), and the percentage of pixels at different intensities of APP signals (F) from control or cholesterol-treated hiPSCs-derived neurons. (5 independent cultures).

(G) 3D plot of ToF-SIMS images from control or MβCD-treated hiPSCs-derived neurons. The y axis indicates the intensity of the pixel. (a.u.).

(H and I) Pixel counts for APP normalized by total counts (H) and the percentage of pixels at different intensities of APP signals (I) from control or MβCD-treated hiPSCs-derived neurons. (6 independent cultures).

(J) Heatmap of ToF-SIMS images for APP co-localized with the cholesterol in control or cholesterol-treated hiPSCs-derived neurons. Scale bar, 5 μm.

(legend continued on next page)

expansion of the signal-positive area but increased density in certain areas (Figure 2F). In contrast, MβCD-treated neurons displayed reduced membrane APP signals in human neurons (Figures 2G–2I). The colocalization analysis showed that the APP and cholesterol colocalization area was expanded in cells treated with cholesterol but shrunken in cells treated with MβCD (Figures 2J–2M).

Astrocyte ApoE4 increases APP expression in the lipid raft domains in human neurons

We have previously shown that an oversupply of cholesterol from ApoE4 astrocytes positively regulates APP expression in neuronal membranes and subsequently increases amyloidogenic APP processing.[14] To validate this observation using ToF-SIMS and examine the potential contribution of neuronal ApoE4 to membrane-specific APP upregulation, we used the current tool for imaging APPs in the lipid rafts of ApoE4 neurons cultured in either ApoE3 ACM or ApoE4 ACM. ApoE3 neurons were also cultured in ApoE3 ACM as a control (Figure 3A). To eliminate the potential effects of donor variability, we used isogenic ApoE4 hiPSCs that were previously generated by replacing the coding sequence for ApoE3 with ApoE4 (Figure S1A).[20] We observed that both $A\beta_{40}$ and $A\beta_{42}$ levels were not altered in ApoE4 neurons compared to ApoE3 neurons when cultured in ApoE3 ACM, possibly due to their lower maturation compared to the previous study (4 weeks of differentiation in this study vs. 6 weeks in the previous study) (Figure 3B). Consistent with the previous study,[14] neurons treated with ApoE4 ACM significantly increased the secretion levels of $A\beta_{42}$ (Figure 3B).

Cells were then subjected to ToF-SIMS imaging, and we observed that cholesterol and APP signals were comparable between ApoE3 and ApoE4 neurons cultured in ApoE3 ACM (Figures 3C–3E). This suggests that neuronal ApoE4 does not affect the levels of lipid rafts or membrane-bound APPs in neurons; therefore, Aβ secretion is not affected (Figure 3B). In contrast, ApoE4 neurons cultured in ApoE4 ACM displayed increased signals for membrane cholesterol and APP compared to those cultured in ApoE3 ACM (Figures 3C–3E). These data suggest that ApoE4 astrocytes positively regulate neuronal lipid rafts and APP expression in the membrane, possibly by increasing extracellular cholesterol levels (Figure S2J), as also reported previously.[11,14] We did not observe any difference in the size of the cells subjected to analysis among the experimental groups (Figures S2K and S2L) Plotting the distribution of the percentage of pixel number as a function of signal intensity showed that changes in cholesterol and APP signals in ApoE4 ACM-treated ApoE4 neurons were caused not only by an expansion of the signal-positive area but also by an increased density of signals (Figures 3F and 3G). Although ApoE4 ACM increased the colocalization area of APP and cholesterol, the correlation between APP expression and cholesterol levels was not altered, as evidenced by the lack of difference in the index of intensity difference among groups (Figures 3H–3J).

As increased levels of the cholesterol-rich domain due to mutations causing familial AD (fAD) have been reported,[11,19] we utilized another isogenic line that we previously generated, in which the Swedish mutant (APP KM670/671NL; APPswe) was introduced into a healthy hiPSCs line[21] (Figure S1A). We used this to determine the effects of the fAD-associated mutation on neuronal lipid rafts by ToF-SIMS imaging (Figure 3A). We found that APPswe mutation in neurons did not affect either cholesterol or APP levels in the membrane (Figures 3C–3E), although it significantly upregulated the secretion of $A\beta_{40}$ and $A\beta_{42}$ (Figure 3B). To determine whether astrocyte APPswe plays a role in regulating neuronal lipid rafts similar to ApoE4 astrocytes, we cultured APPswe neurons in APPswe ACM and subjected them to ToF-SIMS imaging (Figure S2M). Unlike ApoE4 astrocytes, we did not observe a regulatory effect of astrocyte APPswe on cholesterol and APP levels in neuronal membranes (Figures S2P–S2V). These data suggest that astrocyte ApoE4 can induce the upregulation of neuronal $A\beta_{42}$ by expanding the lipid raft domain and APP localization to the rafts, whereas APPswe mutation in neurons does so in a rafts-independent manner.

To validate our observations, we used additional isogenic pairs for ApoE4 and APPswe. We obtained a reference hiPSCs line (KOLF2.1J) recently announced by the iPSC Neurodegenerative Disease Initiative (iNDI) from the NIH's Center for Alzheimer's and Related Dementias (CARD)[22] and its isogenic ApoE4 hiPSCs line generated from the Jackson Laboratory (Figure S1A). We also generated an additional isogenic APPswe line from healthy hiPSCs using CRISPR-Cas9 genome editing (Figure S1A). With these additional ApoE4 and APPswe isogenic lines, we confirmed neuronal APPswe- or astrocyte ApoE4-dependent increase in amyloidogenic APP processing, and lipid raft expansion and APP translocation to the rafts were only ApoE4-specific (Figure S3).

Inhibition of clathrin-dependent endocytosis did not affect ApoE4 ACM-induced $A\beta_{42}$ upregulation

As ApoE4 ACM positively regulates APP expression in lipid rafts, we speculated that it could facilitate amyloidogenic APP processing in a clathrin-independent manner, such as through an increase in the chance of being processed by β- and γ-secretase in the raft,[23,24] or different types of endocytosis including caveolae-mediated endocytosis.[25] To address this, ApoE4 neurons cultured in ApoE4 ACM were treated with dynasore, an inhibitor of dynamin, to block clathrin-mediated endocytosis (Figure 4A). Although APP translocation to endosomes following β- and γ-secretase-dependent cleavage is known to be primary for the amyloidogenic processing of APP, we did not observe an inhibitory effect of dynasore treatment on ApoE4 ACM-induced $A\beta_{42}$ upregulation in ApoE4 neurons, suggesting that astrocyte ApoE4-induced $A\beta_{42}$ production is

(K) The colocalization area of cholesterol and APP was normalized by cell size. (5 independent cultures).
(L) Heatmap of ToF-SIMS images for APP co-localized with the cholesterol in control or MβCD-treated hiPSCs-derived neurons. Scale bar, 5 μm.
(M) The colocalization area of cholesterol and APP was normalized by cell size. (6 independent cultures).
*$p < 0.05$, **$p < 0.01$, ***$p < 0.001$; ns, not significant. (unpaired t test) Error bars represent SEM.

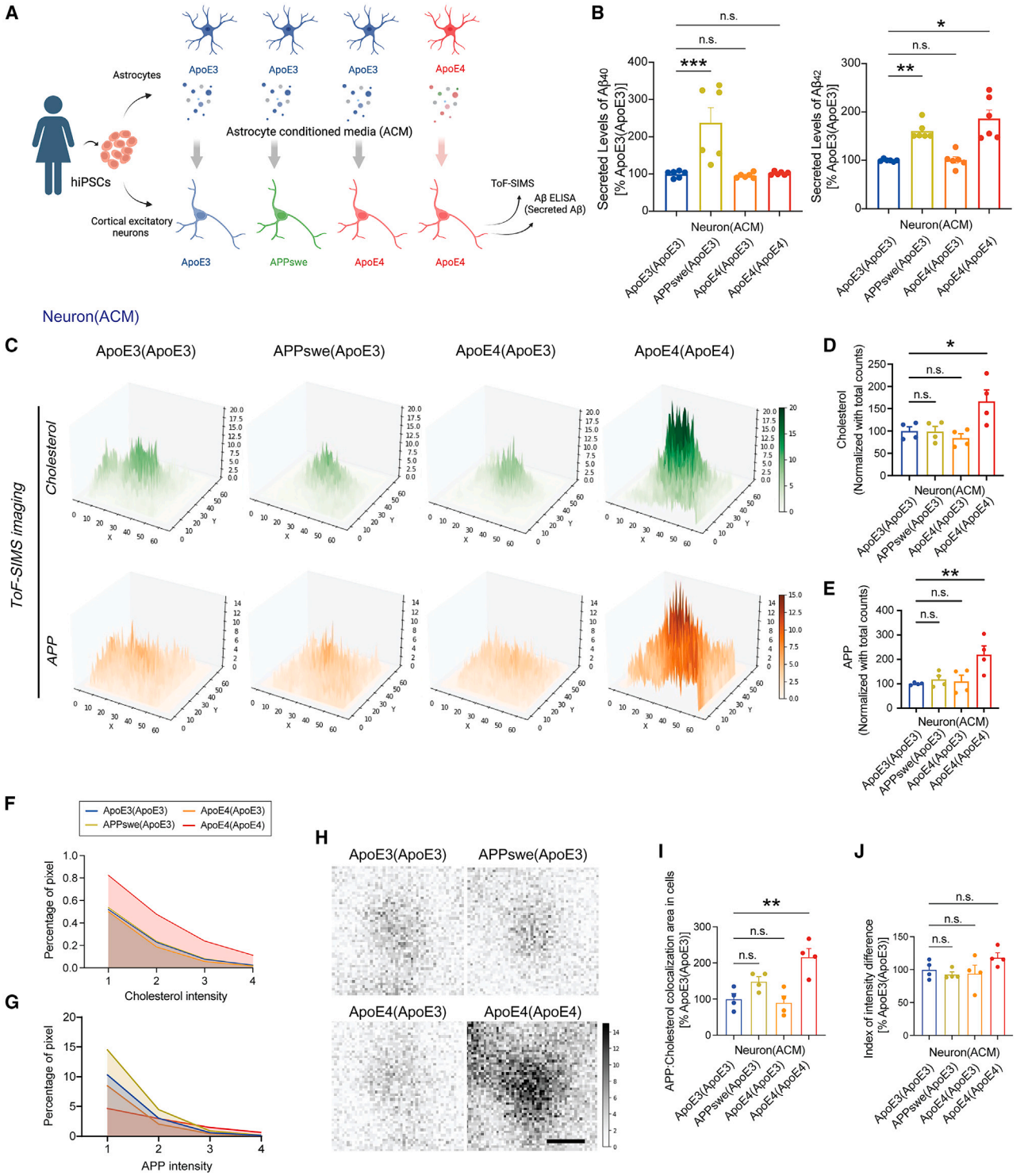

Figure 3. Astrocyte ApoE4 increases APP expression in lipid raft domains in human neurons

(A) Schematics for the experiments to determine the effects of APPswe or ApoE4 on APP processing and lipid rafts.

(B) Levels of secreted $A\beta_{40}$ and $A\beta_{42}$ from neurons were measured by ELISA. (6 independent cultures).

(C) 3D plot of ToF-SIMS images from ApoE3, APPswe, or ApoE4 neurons cultured in either ApoE3 or ApoE4 ACM. The y axis indicates the intensity of the pixel. (a.u.).

(D) Pixel counts for cholesterol normalized by total counts from ApoE3, APPswe, or ApoE4 neurons cultured in either ApoE3 or ApoE4 ACM. (4 independent cultures).

(legend continued on next page)

clathrin-independent (Figure 4B). ToF-SIMS imaging revealed that the effect of inhibiting clathrin-mediated endocytosis on the expression of cholesterol and APP in the membrane was negligible in ApoE4 neurons (Figures 4C–4E). ELISA and ToF-SIMS analyses of another ApoE3/ApoE4 isogenic pair confirmed these observations except for decreased levels of membrane cholesterol in ApoE4 neurons by dynasore treatment (Figures S4A, S4B, and S4D–S4H).

Unlike neurons cultured with ApoE4 ACM, we observed that $A\beta_{42}$ secretion in APPswe neurons was significantly reduced by dynasore in two independent isogenic pairs (Figures 4C and S4C). These data suggested that APPswe-mediated $A\beta_{42}$ upregulation was largely mediated by clathrin-mediated endocytosis of APP, which was confirmed by an increase in the levels of APPs in the membrane after dynasore treatment (Figures 4I, 4L, 4M, 4Q, 4R, S4I, S4L, S4M, S4Q, and S4R). Although we also observed increased levels of cholesterol in the membrane in dynasore-treated APPswe neurons, possibly associated with APP accumulation (Figures 4I–4K, 4Q, 4R, S4I–S4K, S4Q, and S4R), it did not result in $A\beta_{42}$ upregulation. We confirmed that none of the conditions caused a change in the cell size (Figures S4T–S4W). Altogether, our data revealed distinct mechanisms for inducing amyloidogenic APP processing by ApoE4 compared to APPswe mutation in neurons.

DISCUSSION

In a previous study, we successfully imaged cholesterol in the wet membrane of live cells and identified cholesterol-enriched regions.[7] In this study, we provide the methodology to inspect lipid rafts by co-imaging these regions with flotillin-1, a membrane protein predominantly expressed in lipid rafts. The fixation step often disrupts the membrane integrity, thereby generating cracks. Additionally, delayed imaging disintegrates cholesterol-rich signals. However, fixing cells is inevitable when imaging proteins at high resolution. By excluding the permeabilization step, replacing the graphene covering with plasma cleaning, and removing carbohydrates that potentially distract signals from ODs by glycosidases, we obtained clear images of both lipids and QD-conjugated proteins in the plasma membrane without any cracks observed by TEM imaging or diffused signals of cholesterol by ToF-SIMS imaging. For single-cell analysis of lipids and proteins on the plasma membrane, we imaged a 38.4 × 38.4 μm^2 area with 128 × 128 pixels; one pixel corresponds to 300 nm. Although ToF-SIMS was operated in the spectrometry mode with a beam size of 3 μm, the signal in each pixel represents the change of signal from the target measured within 600 nm (the area of 3 μm was imaged with shifting every 300 nm). It potentially includes several lipid rafts, which are difficult to estimate exactly as the size of lipid rafts varies, and we still lack information on the exact distance between lipid rafts. Nonetheless, our 3D construction for the expression of lipids and proteins on the plasma membrane from ToF-SIMS imaging showed the differential intensity of the signals across the pixels and regulated by the treatment of cholesterol or MβCD, proving the value of the current protocol in measuring the dynamics of lipid rafts.

By developing and utilizing a protocol for co-imaging lipids and membrane proteins at a single-cell resolution that allows the investigation of the interaction of lipids and proteins in cell membranes under various conditions, we suggest the context-dependent contribution of lipid raft-dependent APP processing.

Limitations of the study

In this study, although our data are from the isogenic ApoE3/ApoE4 iPSCs in which have been previously validated for minimal off-target effect and shown to effectively recapitulate ApoE4-mediated pathology when differentiated into various brain cell types,[20,26,27] these results could still be donor specific. Therefore, we further used an additional ApoE3 hiPSCs line established as a reference line from iPSC Neurodegenerative Disease Initiative (iNDI)[22] and its isogenic ApoE4 counterpart to validate our observations. For APPswe-carrying iPSCs, we also used two independent isogenic pairs. However, validating these findings across more isogenic pairs would further strengthen the reliability of our results.

As previously reported, the inhibition of APP endocytosis resulted in the accumulation of APPs on the cell surface.[28] Although dynasore treatment significantly reduced $A\beta_{42}$ generation in APPswe neurons, suggesting that facilitated clathrin-dependent APP endocytosis to endosome and subsequent APP processing is the major source of $A\beta_{42}$ overproduction by APPswe mutation, we observed that it also increased the levels of membrane cholesterol. This suggests that the upregulation of membrane APP and cholesterol does not always lead to $A\beta_{42}$ upregulation. Changes in cholesterol content on the membrane induce biophysical changes in terms of microviscosity. These physical environmental changes in the membrane were shown to directly influence the interaction between APP and BACE1, as observed in APP/PSEN1 transgenic mice and the human AD cortex, even in the early stages of the disease.[12,13] Therefore, it would be required to address whether the proximity between APPs and APP cleaving enzymes, BACE1 and γ-secretase, are differentially affected in neurons cultured in ApoE4 ACM and

(E) Pixel counts for APP normalized by total counts from ApoE3, APPswe, or ApoE4 neurons cultured in either ApoE3 or ApoE4 ACM. (4 independent cultures).
(F) The percentage of pixels at different intensities of cholesterol signals from ApoE3, APPswe, or ApoE4 neurons cultured in either ApoE3 or ApoE4 ACM. (4 independent cultures).
(G) The percentage of pixels at different intensities of APP signals from ApoE3, APPswe, or ApoE4 neurons cultured in either ApoE3 or ApoE4 ACM. (4 independent cultures).
(H) Heatmap of ToF-SIMS images for APP co-localized with the cholesterol in ApoE3, APPswe, or ApoE4 neurons cultured in either ApoE3 or ApoE4 ACM. Scale bar, 5 μm.
(I) The colocalization area of cholesterol and APP was normalized by cell size. (4 independent cultures).
(J) The Index of intensity difference for cholesterol and APP was calculated from ApoE3, APPswe, or ApoE4 neurons cultured in either ApoE3 or ApoE4 ACM. (4 independent cultures).
*$p < 0.05$, **$p < 0.01$, ***$p < 0.001$; ns, not significant. (one-way ANOVA test followed by Dunnett's multiple comparison analysis). Error bars represent SEM.

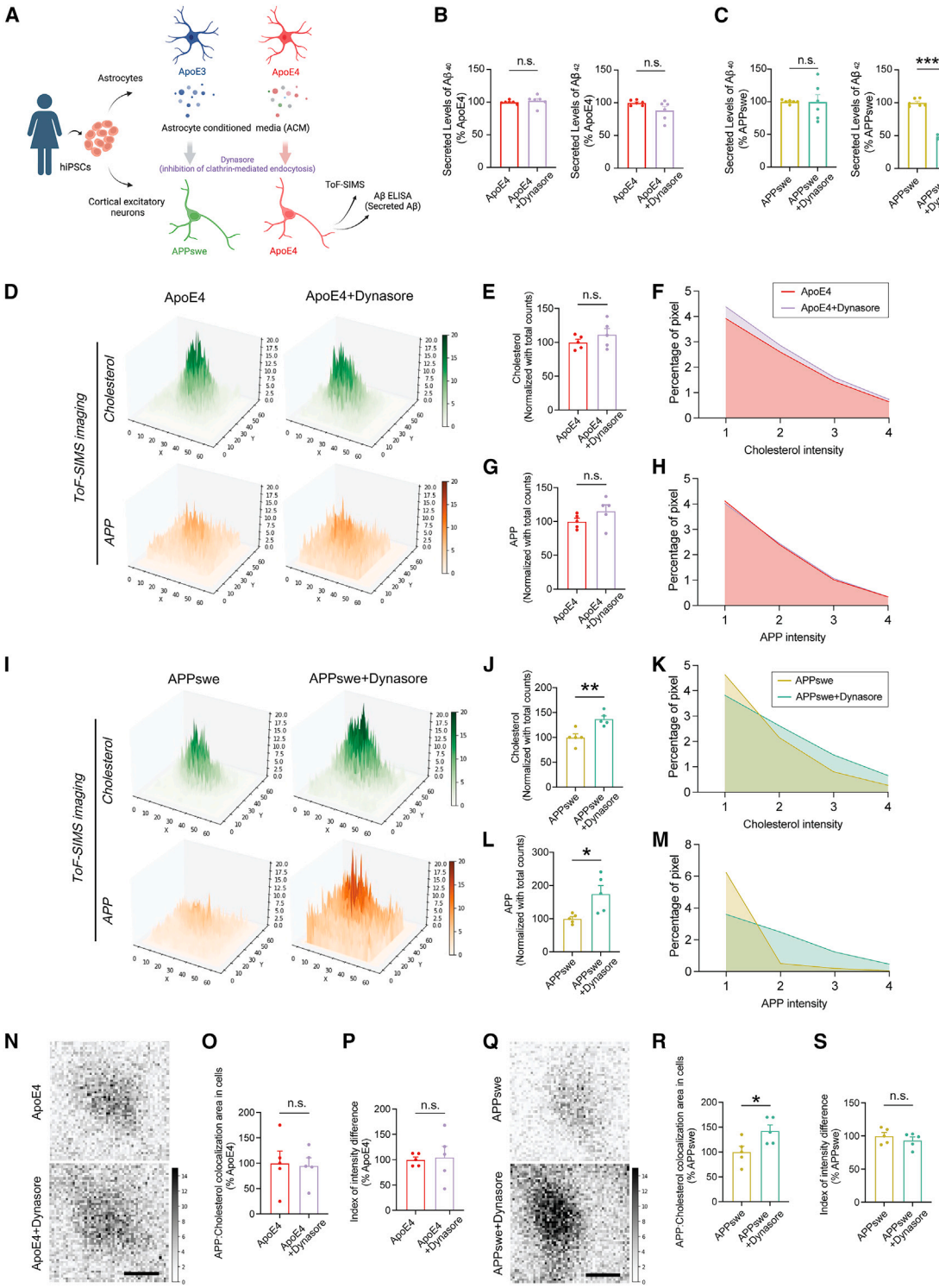

Figure 4. Astrocyte ApoE4-induced amyloidogenic APP processing is clathrin-mediated endocytosis independent

(A) Schematics for the experiments to determine the effects of inhibition of clathrin-mediated endocytosis on ApoE4-induced amyloidogenic APP processing.

(B and C) Levels of secreted $A\beta_{40}$ and $A\beta_{42}$ from neurons were measured by ELISA. (6 independent cultures).

(D) 3D plot of ToF-SIMS images from ApoE4 neurons cultured in ApoE4 ACM with or without dynasore treatment. The y axis indicates the intensity of the pixel. (a.u.).

(legend continued on next page)

dynasore-treated APPswe neurons, both of which show increased levels of membrane cholesterol and APP.

Consequently, our findings suggest that alterations in APP processing due to lipid raft expansion within the neuronal membrane could lead to Aβ upregulation, potentially contributing to AD pathology and highlighting the importance of developing tailored therapeutics targeting these specific causal factors.

RESOURCE AVAILABILITY

Lead contact

Further requests for the resources and reagents should be directed to and will be fulfilled by the lead contact, Jinsoo Seo (jsseo@dgist.ac.kr).

Materials availability

All unique materials and reagents will be available from the lead contact with a completed materials transfer agreement upon reasonable request.

Data and code availability

- All data reported in this article will be shared by the lead contact upon request.
- This article does not report the original code.
- Any additional information required to reanalyze the data reported in this article is available from the lead contact upon request.

ACKNOWLEDGMENTS

The authors would like to thank all members of Seo lab for their advice and discussion. We also thank Dr. Tsai at MIT and Dr. Yankner at Harvard Medical School for sharing their iPSCs lines. This work was supported by the National Research Foundation of Korea (NRF) grants funded by the Ministry of Science and ICT (MSIT), South Korea (2021R1C1C2010928 to H.L, 2021R1A2C1008704 to D.W.M, 2022R1A4A2000703 and 2022R1A2C4001611 to J.S.). All schematics and a graphical abstract were created using BioRender with a full license to publish.

AUTHOR CONTRIBUTIONS

S.-I.L, H.L, D.W.M., and J.S. designed the research, S.-I.L., H.L., N.Y.K., J.Y., J.C., and H.L. performed research and analyzed the data, and S.-I.L, H.L, D.W.M., and J.S. wrote the manuscript.

DECLARATION OF INTERESTS

The authors declare no competing interests.

STAR★METHODS

Detailed methods are provided in the online version of this paper and include the following:

- KEY RESOURCES TABLE
- EXPERIMENTAL MODEL AND STUDY PARTICIPANT DETAILS
  - iPSCs lines
- METHOD DETAILS
  - Generation of APPswe isogenic hiPSCs line
  - Cortical excitatory neurons differentiation from hiPSCs
  - Astrocytes differentiation from hiPSCs
  - Preparation of antibody-biotin-streptavidin-QD complex
  - Time-of-flight secondary ion mass spectrometry (ToF-SIMS) imaging
  - Transmission electron microscopy (TEM) imaging
  - Confocal imaging
  - Drug treatment
  - ELISA
  - Cholesterol-Glo assay
- QUANTIFICATION AND STATISTICAL ANALYSIS

SUPPLEMENTAL INFORMATION

Supplemental information can be found online at https://doi.org/10.1016/j.isci.2025.111893.

Received: September 11, 2024
Revised: December 1, 2024
Accepted: January 22, 2025
Published: January 25, 2025

REFERENCES

1. Singer, S.J., and Nicolson, G.L. (1972). The Fluid Mosaic Model of the Structure of Cell Membranes. Science *175*, 720–731. https://doi.org/10.1126/science.175.4023.720.
2. Yu, J., Fischman, D.A., and Steck, T.L. (1973). Selective solubilization of proteins and phospholipids from red blood cell membranes by nonionic

(E and F) Pixel counts for cholesterol normalized by total counts (E) and the percentage of pixels at different intensities of cholesterol signals (F) from ApoE4 neurons cultured in ApoE4 ACM with or without dynasore treatment. (5 independent cultures).
(G and H) Pixel counts for APP normalized by total counts (G), and the percentage of pixels at different intensities of APP signals (H) from ApoE4 neurons cultured in ApoE4 ACM with or without dynasore treatment. (5 independent cultures).
(I) 3D plot of ToF-SIMS images from APPswe neurons cultured in ApoE3 ACM with or without dynasore treatment. The y axis indicates the intensity of the pixel. (a.u.).
(J and K) Pixel counts for cholesterol normalized by total counts (J) and the percentage of pixels at different intensities of cholesterol signals (K) from APPswe neurons cultured in ApoE3 ACM with or without dynasore treatment. (5 independent cultures).
(L and M) Pixel counts for APP normalized by total counts (L) and the percentage of pixels at different intensities of APP signals (M) from APPswe neurons cultured in ApoE3 ACM with or without dynasore treatment. (5 independent cultures).
(N) Heatmap of ToF-SIMS images for APP co-localized with the cholesterol from ApoE4 neurons cultured in ApoE4 ACM with or without dynasore treatment. Scale bar, 5 μm.
(O) The colocalization area of cholesterol and APP was normalized by cell size. (5 independent cultures).
(P) The Index of intensity difference for cholesterol and APP was calculated from ApoE4 neurons cultured in ApoE4 ACM with or without dynasore treatment. (5 independent cultures).
(Q) Heatmap of ToF-SIMS images for APP co-localized with the cholesterol from APPswe neurons cultured in ApoE3 ACM with or without dynasore treatment. Scale bar, 5 μm.
(R) The colocalization area of cholesterol and APP was normalized by cell size. (5 independent cultures).
(S) The Index of intensity difference for cholesterol and APP was calculated from APPswe neurons cultured in ApoE3 ACM with or without dynasore treatment. (5 independent cultures).
$^{*}p < 0.05$, $^{**}p < 0.01$, $^{****}p < 0.0001$; ns, not significant. (unpaired t test) Error bars represent SEM.

detergents. J. Supramol. Struct. *1*, 233–248. https://doi.org/10.1002/jss.400010308.

3. Pike, L.J. (2003). Lipid rafts: bringing order to chaos. J. Lipid Res. *44*, 655–667. https://doi.org/10.1194/jlr.r200021-jlr200.
4. Sezgin, E., Levental, I., Mayor, S., and Eggeling, C. (2017). The mystery of membrane organization: composition, regulation and roles of lipid rafts. Nat. Rev. Mol. Cell Biol. *18*, 361–374. https://doi.org/10.1038/nrm.2017.16.
5. Pike, L.J. (2006). Rafts defined: a report on the Keystone symposium on lipid rafts and cell function. J. Lipid Res. *47*, 1597–1598. https://doi.org/10.1194/jlr.e600002-jlr200.
6. Oh, S., Lee, C., Yang, W., Li, A., Mukherjee, A., Basan, M., Ran, C., Yin, W., Tabin, C.J., Fu, D., et al. (2022). Protein and lipid mass concentration measurement in tissues by stimulated Raman scattering microscopy. Proc. Natl. Acad. Sci. USA *119*, e2117938119. https://doi.org/10.1073/pnas.2117938119.
7. Lim, H., Lee, S.Y., Park, Y., Jin, H., Seo, D., Jang, Y.H., and Moon, D.W. (2021). Mass spectrometry imaging of untreated wet cell membranes in solution using single-layer graphene. Nat. Methods *18*, 316–320. https://doi.org/10.1038/s41592-020-01055-6.
8. Filipp, D., Leung, B.L., Zhang, J., Veillette, A., and Julius, M. (2004). Enrichment of lck in lipid rafts regulates colocalized fyn activation and the initiation of proximal signals through TCR alpha beta. J. Immunol. *172*, 4266–4274. https://doi.org/10.4049/jimmunol.172.7.4266.
9. Cordy, J.M., Hussain, I., Dingwall, C., Hooper, N.M., and Turner, A.J. (2003). Exclusively targeting β-secretase to lipid rafts by GPI-anchor addition up-regulates β-site processing of the amyloid precursor protein. Proc. Natl. Acad. Sci. USA *100*, 11735–11740. https://doi.org/10.1073/pnas.1635130100.
10. Bhattacharyya, R., Barren, C., and Kovacs, D.M. (2013). Palmitoylation of Amyloid Precursor Protein Regulates Amyloidogenic Processing in Lipid Rafts. J. Neurosci. *33*, 11169–11183. https://doi.org/10.1523/jneurosci.4704-12.2013.
11. Wang, H., Kulas, J.A., Wang, C., Holtzman, D.M., Ferris, H.A., and Hansen, S.B. (2021). Regulation of beta-amyloid production in neurons by astrocyte-derived cholesterol. Proc. Natl. Acad. Sci. USA *118*, e2102191118. https://doi.org/10.1073/pnas.2102191118.
12. Fabelo, N., Martín, V., Marín, R., Moreno, D., Ferrer, I., and Díaz, M. (2014). Altered lipid composition in cortical lipid rafts occurs at early stages of sporadic Alzheimer's disease and facilitates APP/BACE1 interactions. Neurobiol. Aging *35*, 1801–1812. https://doi.org/10.1016/j.neurobiolaging.2014.02.005.
13. Díaz, M., Fabelo, N., Martín, V., Ferrer, I., Gómez, T., and Marín, R. (2014). Biophysical Alterations in Lipid Rafts from Human Cerebral Cortex Associate with Increased BACE1/AβPP Interaction in Early Stages of Alzheimer's Disease. J. Alzheimer's Dis. *43*, 1185–1198. https://doi.org/10.3233/jad-141146.
14. Lee, S.-I., Jeong, W., Lim, H., Cho, S., Lee, H., Jang, Y., Cho, J., Bae, S., Lin, Y.-T., Tsai, L.-H., et al. (2021). APOE4-carrying human astrocytes oversupply cholesterol to promote neuronal lipid raft expansion and Aβ generation. Stem Cell Rep. *16*, 2128–2137. https://doi.org/10.1016/j.stemcr.2021.07.017.
15. Dermine, J.-F., Duclos, S., Garin, J., St-Louis, F., Rea, S., Parton, R.G., and Desjardins, M. (2001). Flotillin-1-enriched Lipid Raft Domains Accumulate on Maturing Phagosomes. J. Biol. Chem. *276*, 18507–18512. https://doi.org/10.1074/jbc.m101113200.
16. Moon, D.W., Park, Y.H., Lee, S.Y., Lim, H., Kwak, S., Kim, M.S., Kim, H., Kim, E., Jung, Y., Hoe, H.-S., et al. (2020). Multiplex Protein Imaging with Secondary Ion Mass Spectrometry Using Metal Oxide Nanoparticle-Conjugated Antibodies. Acs. Appl. Mater Inter. *12*, 18056–18064. https://doi.org/10.1021/acsami.9b21800.
17. Deerinck, T.J. (2008). The Application of Fluorescent Quantum Dots to Confocal, Multiphoton, and Electron Microscopic Imaging. Toxicol. Pathol. *36*, 112–116. https://doi.org/10.1177/0192623307310950.
18. Simons, K., and Ehehalt, R. (2002). Cholesterol, lipid rafts, and disease. J. Clin. Invest. *110*, 597–603. https://doi.org/10.1172/jci16390.
19. Cho, Y.Y., Kwon, O.-H., Park, M.K., Kim, T.-W., and Chung, S. (2019). Elevated cellular cholesterol in Familial Alzheimer's presenilin 1 mutation is associated with lipid raft localization of β-amyloid precursor protein. PLoS One *14*, e0210535. https://doi.org/10.1371/journal.pone.0210535.
20. Lin, Y.-T., Seo, J., Gao, F., Feldman, H.M., Wen, H.-L., Penney, J., Cam, H.P., Gjoneska, E., Raja, W.K., Cheng, J., et al. (2018). APOE4 Causes Widespread Molecular and Cellular Alterations Associated with Alzheimer's Disease Phenotypes in Human iPSC-Derived Brain Cell Types. Neuron *98*, 1141–1154.e7. https://doi.org/10.1016/j.neuron.2018.05.008.
21. Park, J.-H., Hwang, J.-W., Lee, H.J., Jang, G.M., Jeong, Y.J., Cho, J., Seo, J., and Hoe, H.-S. (2023). Lomerizine inhibits LPS-mediated neuroinflammation and tau hyperphosphorylation by modulating NLRP3, DYRK1A, and GSK3α/β. Front. Immunol. *14*, 1150940. https://doi.org/10.3389/fimmu.2023.1150940.
22. Pantazis, C.B., Yang, A., Lara, E., McDonough, J.A., Blauwendraat, C., Peng, L., Oguro, H., Kanaujiya, J., Zou, J., Sebesta, D., et al. (2022). A reference human induced pluripotent stem cell line for large-scale collaborative studies. Cell Stem Cell *29*, 1685–1702.e22. https://doi.org/10.1016/j.stem.2022.11.004.
23. Hicks, D.A., Nalivaeva, N.N., and Turner, A.J. (2012). Lipid Rafts and Alzheimer's Disease: Protein-Lipid Interactions and Perturbation of Signaling. Front. Physiol. *3*, 189. https://doi.org/10.3389/fphys.2012.00189.
24. Vetrivel, K.S., Cheng, H., Lin, W., Sakurai, T., Li, T., Nukina, N., Wong, P.C., Xu, H., and Thinakaran, G. (2004). Association of γ-Secretase with Lipid Rafts in Post-Golgi and Endosome Membranes. J. Biol. Chem. *279*, 44945–44954. https://doi.org/10.1074/jbc.m407986200.
25. El-Sayed, A., and Harashima, H. (2013). Endocytosis of Gene Delivery Vectors: From Clathrin-dependent to Lipid Raft-mediated Endocytosis. Mol. Ther. *21*, 1118–1130. https://doi.org/10.1038/mt.2013.54.
26. Victor, M.B., Leary, N., Luna, X., Meharena, H.S., Scannail, A.N., Bozzelli, P.L., Samaan, G., Murdock, M.H., von Maydell, D., Effenberger, A.H., et al. (2022). Lipid accumulation induced by APOE4 impairs microglial surveillance of neuronal-network activity. Cell Stem Cell *29*, 1197–1212.e8. https://doi.org/10.1016/j.stem.2022.07.005.
27. Sienski, G., Narayan, P., Bonner, J.M., Kory, N., Boland, S., Arczewska, A.A., Ralvenius, W.T., Akay, L., Lockshin, E., He, L., et al. (2021). APOE4 disrupts intracellular lipid homeostasis in human iPSC-derived glia. Sci. Transl. Med. *13*, eaaz4564. https://doi.org/10.1126/scitranslmed.aaz4564.
28. Cirrito, J.R., Kang, J.-E., Lee, J., Stewart, F.R., Verges, D.K., Silverio, L.M., Bu, G., Mennerick, S., and Holtzman, D.M. (2008). Endocytosis Is Required for Synaptic Activity-Dependent Release of Amyloid-β In Vivo. Neuron *58*, 42–51. https://doi.org/10.1016/j.neuron.2008.02.003.

STAR★METHODS

KEY RESOURCES TABLE

REAGENT or RESOURCE	SOURCE	IDENTIFIER
Antibodies		
Anti-AQP4 antibody	Sigma-Aldrich	Cat#SAB5200112
Anti-ALDH1L1 antibody (YY8)	Santa Cruz Biotechnology	Cat#sc-100497, RRID:AB_2224180
Anti-PSD-95 antibody	Thermo Fischer Scientific	Cat#MA1045, RRID:AB_325399
Anti-Synapsin antibody	Cell Signaling Technology	Cat#5297, RRID:AB_2616578
Anti-Flotillin-1 antibody	Abcam	Cat#ab41927, RRID:AB_941621
Anti-APP antibody	Abcam	Cat#ab126732, RRID:AB_11131727
Anti-MFN1 antibody	Santa Cruz Biotechnology	Cat#sc-166644, RRID:AB_2142616
Anti-BACE1 antibody	Thermo Fischer Scientific	Cat#MA1177, RRID:AB_2608440
Anti-GLAST-PE antibody	Miltenyi Biotec	Cat#130-118-344 RRID:AB_2733723
Chemicals, peptides, and recombinant proteins		
DMEM/F12, GlutaMAX supplement	Gibco	Cat#10565-018
hESC-qualified Matrigel	Corning	Cat#356277
MEM Non-Essential Amino Acids Solution	Gibco	Cat#11140-050
N-2	Gibco	Cat#17504-044
Recombinant human BDNF	PeproTech	Cat#450-02
Recombinant human NT-3	PeproTech	Cat#450-03
Laminin	Corning	Cat#354232
B-27	Gibco	Cat#10565-018
GlutaMAX	Gibco	Cat#35050-061
Puromycin	Millipore	Cat#5.08838.0001
Ara-C	Sigma-Aldrich	Cat#C1768
Insulin	Sigma-Aldrich	Cat#19278
2-mercaptoethanol	Sigma-Aldrich	Cat#M6250
Penicillin/ Streptomycin	Gibco	Cat#15140122
Astrocyte Medium	ScienCell	Cat#1801
Dorsomorphin	Tocris	Cat#3093
SB431542	Tocris	Cat#1614
NeutrAvidin Resins	Thermo Fisher Scientific	Cat#29202
4x sample buffer	Bio-Rad	Cat#1610747
Polyvinylidene difluoride membrane	Bio-Rad	Cat#1620177
4% paraformaldehyde	Biosesang	Cat#P2031
4% glutaraldehyde	Electron Microscopy Sciences	Cat#16539-60
Recombinant human FGF-basic	PeproTech	Cat#100-18B
Recombinant human BMP-4	PeproTech	Cat#AF-120-05ET
DPBS	Biowest	Cat#L0615-500
Streptavidin-conjugated QD-655	Invitrogen	Cat#Q10121MP
Q-Glycosidase	New England Biolabs	Cat#P0733
PNGase F	Sigma-Aldrich	Cat#P7367
Cholesterol	Calbiochem	Cat#228111
Ammonium acetate	Daejung	Cat#2511-4405
Methyl-β-cyclodextrin	Sigma-Aldrich	Cat#C4555
Dynasore	Sigma-Aldrich	Cat#D7693

(*Continued on next page*)

Continued

REAGENT or RESOURCE	SOURCE	IDENTIFIER
Critical commercial assays		
Amyloid-beta 42 Human ELISA kit	Thermo Fisher Scientific	Cat#KHB3442
Amyloid-beta 40 Human ELISA kit	Thermo Fisher Scientific	Cat#KHB3481
Biotin conjugation kit	Abcam	Cat#ab201795
Cholesterol-Glo	Promega	Cat#J3190
Experimental models: Cell lines		
Human iPSC line from a healthy control (*APOE3*)	Coriell	Cat#AG09173
APOE4 isogenic line from #AG09173	Tsai Laboratory (Lin et al.)[5]	N/A
Human iPSC line from a healthy control (*APOE3*)	The Jackson Laboratory	Cat#JIPC1000
APOE4 isogenic line from #JIPC1000	The Jackson Laboratory	Cat#JIPC1150
Human iPSC line from a healthy control	Coriell	Cat#GM23720
APPswe isogenic line from #GM23720	Seo Laboratory (Park et al.)[21]	N/A
APPswe isogenic line from #AG09173	In this study	N/A
HEK293T	Sigma-Aldrich	Cat#12022001 RRID:CVCL_0063
Recombinant DNA		
pLV-TetO-hNGN2-eGFP-puro	Addgene	Cat#79823, RRID:Addgene_79823
FUdeltaGW-rtTA	Addgene	Cat#19780, RRID:Addgene_19780
Software and algorithms		
Prism 9	GraphPad	RRID:SCR_002798
Spyder	MIT	RRID:SCR_017585
Zen software	Zeiss	RRID:SCR_018163
ImageJ	NIH	RRID:SCR_003070
Other		
Quantifoil holey carbon grid	SPI Supplies	Cat#4430-XA
Single-layered graphene	Graphene Supermarket	Cat#UHC-GO

EXPERIMENTAL MODEL AND STUDY PARTICIPANT DETAILS

iPSCs lines

The use of human iPSCs was approved by the Institutional Review Board (IRB) of Daegu Gyeongbuk Institute for Science and Technology (Permit Number: DGIST-190829-BR-071-01). ApoE3 hiPSCs (Coriell #AG09173, age 75 years, female) were used for the generation of ApoE4 hiPSCs through CRISPR/Cas9 genome editing as previously described.[20] Another ApoE3/E4 isogenic hiPSCs pair was obtained from the Jackson Laboratory (KOLF2.1J, age 55-59 years, male).[22] APPswe isogenic hiPSCs line was generated by the CRISPR/Cas9 genome editing as previously described.[21]

METHOD DETAILS

Generation of APPswe isogenic hiPSCs line

Additional APPswe hiPSCs line was generated from #AG09173 line mentioned above by the CRISPR/Cas9 genome editing with sgRNA (5'-GCAGAATTCCGACATGACTC-3') and ssODN (5'-GTTCTGGGTTGACAAATATCAAGACGGAGGAGATCTCTGAA GTGAATCTCGATGCAGAATTCCGACATGACTCAGGATATGAAGTTCATCATCAAAAATTG-3'). Karyotyping was performed to confirm that genome editing did not cause any chromosome abnormalities.

Cortical excitatory neurons differentiation from hiPSCs

hiPSCs were differentiated into cortical excitatory neurons as previously described.[20] In brief, lentiviruses with pLV-TetO-hNGN2-eGFP-puro and rtTA sequences were applied to hiPSCs for transfection. hiPSCs were then seeded onto a Matrigel-coated 6-well plate at a density of 4 x 10^6 cells/well. The next day, the media were replaced with neuron differentiation media [DMEM/F12 (Gibco), 1x N2(Gibco), 1x NEAA] containing neuron differentiation supplements [10 ng/ml BDNF (Peprotech), 10 ng/ml NT-3 (Peprotech),

0.2 μg/ml laminin (Corning), and 2 μg/ml doxycycline (Sigma-Aldrich)]. After 2 days, the media were completely changed with Neurobasal media (Gibco) containing 1x B27 (Gibco), 1x GlutaMAX (Gibco), 1 μg/ml puromycin (Millipore), and neuron differentiation supplements. Two days later, the cells were seeded onto a Matrigel-coated 24-well plate at a density of 1 x 10^5 cells/well. The next day, media were replaced with ACM with 1 μM Ara-C (Sigma-Aldrich) and neuron differentiation supplements. After that, half of the volume of media was changed with ACM supplemented with neuron differentiation supplements every 4 days.

Astrocytes differentiation from hiPSCs

hiPSCs were differentiated into astrocytes as previously described.[20] In brief, culture media of hiPSCs were replaced with neuronal induction media [DMEM/F-12 GlutaMAX, Neurobasal, 0.5x N-2, 0.5x B27, 5 μg/ml insulin (Sigma-Aldrich), 0.5x NEAA (Thermo Fisher Scientific), 100 μM 2-mercaptoethanol (Sigma-Aldrich), and 1x Penicillin/ Streptomycin (Gibco)] supplemented with 1 μM Dorsomorphin (Tocris) and 10 μM SB431542 (Tocris) to induce neural progenitor cell (NPC) differentiation. After 11 days, the cells were passaged onto a Matrigel-coated 6-well plate and cultured with neuronal induction media. After 4 days, the cells were passaged and cultured with neuronal induction media containing 20 ng/ml FGF2 (Peprotech) to promote the proliferation of NPC. To differentiate NPCs into astrocytes, cells were seeded at a density of 3 x 10^5 cells/well in a Matrigel-coated 6-well plate. The next day, the media were replaced with neuronal induction media containing 20 ng/ml FGF2 (Peprotech) and 10 ng/ml BMP4 (Peprotech). The media were replaced with fresh media every 1 or 2 days. After 28 days, astrocytes were collected by sorting cells with an anti-GLAST-PE antibody (Miltenyi Biotec) using a cell sorter (Sony SH800S).

Preparation of antibody-biotin-streptavidin-QD complex

Antibody biotinylation

A Biotin Conjugation kit (Abcam) was used following the manufacturer's instructions. In brief, antibodies were mixed with modifier reagent and transferred to a vial of Biotin Conjugation Mix, followed by incubation in the dark for 15 min. After the incubation, Quencher reagent was added to the biotinylated antibodies.

Pull-down assay

Cell lysates were extracted from HEK 293T cells with RIPA buffer (50 mM Tris pH 8.0, 150 mM NaCl, 1% NP-40, 0.5% sodium deoxycholate, 0.1% SDS). Biotinylated primary antibodies were added to the lysates and rotated at 4°C. The next day, avidin-conjugated agarose beads (Thermo Fisher Scientific) were treated to lysate containing primary antibodies, then rotated at 4°C for 3 hr. After rotating, avidin-conjugated agarose beads were separated from the lysate solution by centrifugation (Eppendorf) at 500 g for 1 min. The separated avidin-conjugated agarose beads were then washed with RIPA buffer three times. A sample buffer (Bio-Rad) was added to avidin-conjugated agarose beads, and then the mixtures were incubated at 98°C for 10 min. The pull-downed samples were subjected to SDS-PAGE and transferred to polyvinylidene difluoride membrane (Bio-Rad) and proved with the indicated antibodies.

Sample preparation for ToF-SIMS imaging

hiPSC-derived neurons were fixed with 4% paraformaldehyde after washing with cold DPBS. After fixation, neurons were washed with cold DPBS twice, treated with biotinylated antibodies diluted with 6% BSA in DPBS at 1:50, and incubated at room temperature for 1 hr. After incubation, neurons were washed with cold DPBS twice and treated with streptavidin-conjugated QD-655 (Invitrogen) at a concentration of 20 nM for 1 hr at room temperature. For removing glycans in the cell membrane, O-Glycosidase (New England Biolabs) and PNGase F (Sigma-Aldrich) were treated in neurons for 1 hr at 37°C. Neurons were washed with cold DPBS twice and fixed with 4% glutaraldehyde (Electron Microscopy Sciences) for 10 min. After fixation, neurons were washed with DPBS and 150 mM ammonium acetate in pure water, dried at room temperature for 20 min, and treated with the air plasma beam (70 W, 50 kHz) for 3 min.

Time-of-flight secondary ion mass spectrometry (ToF-SIMS) imaging

The ToF-SIMS 5-100 equipment (ION-TOF) was utilized for ToF-SIMS imaging analysis using a pulsed 30 keV Bi^{3+} primary ion beam in the spectrometry mode with a beam size of 3 μm. The ToF-SIMS images of positive ions were obtained over a 500 × 500 μm^2 area with 256 × 256 pixels or 38.4 × 38.4 μm^2 area with 128 × 128 pixels. Low-energy electrons were supplied onto the sample surface using an electron flood gun for charging compensation during analysis. Prior to analysis, internal mass calibration for all the ToF-SIMS spectra was performed using the peaks of CH_3^+, Na^+, $C_2H_3^+$, $C_3H_5^{+,}$ and $C_4H_7^+$ for the positive ion mode. The detected ToF-SIMS images were visualized with 3D plot using Python codes and Spyder software (MIT). To calculate the index of intensity difference, we first determined the rank (from 1∼100) of each pixel from cholesterol, flotillin-1, phosphocholine, or APP image based on its signal intensity, then calculated the absolute difference in ranks from two signals compared.

Transmission electron microscopy (TEM) imaging

hiPSC-derived neurons were seeded on a quantifoil holey carbon grid (SPI Supplies). After labeling the target protein with QDs, the grid was covered with single-layered graphene (Graphene Supermarket) and dried for 30 min. TEM imaging analysis of the QD-labelled neurons on the grid was performed on a Tecnai G2 F20 TWIN TMP instrument (FEI) using an accelerating voltage of 200 kV.

Confocal imaging

The LSM 800 confocal microscope (Zeiss) was used for imaging. Zen software (Zeiss) and ImageJ (NIH) were used for data analysis.

Drug treatment

To increase extracellular levels of cholesterol, 20 μM cholesterol (Calbiochem) was applied to neurons for 4 days. To reduce levels of cholesterol, neurons were treated with 600 μM methyl-β-cyclodextrin (MβCD, Sigma-Aldrich) for 24 hr. To inhibit clathrin-mediated endocytosis, 40 μM dynasore (Sigma-Aldrich) was applied to neurons for 24 hr.

ELISA

Levels of secreted $A\beta_{40}$ and $A\beta_{42}$ were measured by human Aβ ELISA kits (Thermo Fisher Scientific). Experimental procedures followed the manufacturer's instructions. The microplate reader FlexStation 3 (Molecular Devices) was used to measure the absorbance at a wavelength of 450 nm.

Cholesterol-Glo assay

Cholesterol-Glo assay kit (Promega) was used to examine the levels of total cholesterol in ACM based on the manufacturer's instructions. An equal number of astrocytes from each condition was confirmed by CellTiter-Glo assay (Promega).

QUANTIFICATION AND STATISTICAL ANALYSIS

Pearson's correlation coefficient analysis, unpaired t-test, Mann-Whitney test, or one-way ANOVA test followed by Dunnett's multiple comparison analysis was performed using Prism10 (Graph Pad) software. All of the statistical details of experiments can be found in the figure legends.